Spatial coherence of a Raman wake excited inside a uniform filament

Roman V. Volkov* and Andrey B. Savel'ev
Physics Department and International Laser Centre of M. V. Lomonosov Moscow State University, Vorob'evy Gory 1/62, Moscow 119991, Russia
(Received 11 May 2015; published 14 September 2015)

We present results of an investigation of the spatial-temporal structure of the delayed Kerr nonlinearity excited during filamentation of a femtosecond laser pulse inside a crystalline target. It is found that the pulse splitting, which is an inherent property of the filamentation process, constrains the length of the spatial coherence of the Raman wake wave which follows the pump pulse. Each subpulse induces lattice vibrations, which interfere either constructively or destructively depending on the delay between the subpulses. This results in abrupt "switching" of the phase of the wake wave along and across the filament volume. For the same reason, the maximal amplitude of the Raman response is observed not at the point of the maximal laser intensity and electron concentration—it is shifted forward to the end of the filament. This effect should be observed if the period of Raman oscillations is close to the duration of the pump pulse.

DOI: 10.1103/PhysRevA.92.033820 PACS number(s): 42.65.Re, 42.65.Jx, 42.65.Dr

I. INTRODUCTION

The phenomenon of filamentation of laser radiation has found a wide area of applications in laser physics [1]. Although it was discovered almost four decades ago [2], it is still a subject of extensive investigation. It has been found that filamentation is accompanied by processes, such as plasma generation, self-phase modulation, four-wave mixing, etc. [1–6]. If filamentation occurs in the media with Raman nonlinearity the delayed response can play an important role in the spatial and temporal dynamics of femtosecond radiation. A rotational response of diatomic molecules excited during filamentation in air has been comprehensively investigated (see, e.g., [7–15]). In particular, the presence of a molecular alignment wake following a pump pulse has been revealed. This wake can structure the nonlinearity of the media [9] and has a strong effect on the propagation dynamics of a probe pulse, specifically on its temporal and spectral characteristics [10–14]. The extent of this influence dramatically depends on the delay between the pump and the probe pulses [10–14]. If the trailing pulse is strong enough, it in turn can coherently amplify or dampen the molecular rotational response induced by the leading pulse [14,15].

A similar picture of the two pulses interacting through the delayed nonlinearity should exist during filamentation, even of a single pulse. In this case the roles of leading and trailing radiation should play subpulses which originate from the splitting of the pump pulse [1]. As the delay between the subpulses gradually changes with time, the trailing subpulse should either amplify or dampen the Raman oscillations induced by the leading one while they propagate along the filament. This should result in a spatial modulation of the parameters of the excited Raman wake wave. As the maximal delay between the subpulses is comparable with the pump pulse duration [1], such an effect should be observed if the initial pump pulse duration is comparable with the period of Raman oscillations of the media.

In this study we investigated the spatial distribution over the filament volume of both the amplitude and the phase of a vibrational wake wave induced during filamentation of a single femtosecond pulse in a crystalline target. For this purpose, the angular resolved spectra (ARS) of a delayed weak probe pulse, which is scattered by these vibrations, are measured and compared with the calculated ones.

II. EXPERIMENT

The experiments were performed using a Ti:sapphire laser system delivering 800-nm, 50-fs pulses at 10 Hz. The full width at half maximum (FWHM) diameter of the output beam was about 7 mm. The radiation was split into two parts (Fig. 1). The frequency of one part was doubled by a 0.25-mm-thick type I BBO crystal and was used for probing. The energy of the probe pulse at the second harmonic (SH) was about 0.2 μJ. The pump and probe pulses were brought together by a dielectric mirror to accomplish the collinear probing scheme. Both pulses were focused into the 5-mm-thick KH_2PO_4 crystal (KDP) by a 100-cm focal length aluminum mirror. The KDP crystal was used as a target because its most intense lattice vibration mode has a period of about 36 fs [16]—comparable with the pump pulse duration. The FWHM diameter of the pump and the probe pulses at the entrance facet were 90 and 45 μm, respectively. The 400-nm probe pulse radiation was an extraordinary wave (e wave) and the 800-nm pump pulse radiation was an ordinary wave (o wave). The KDP crystal was oriented so that the angle θ between the laser beams and the optical (z) axis of the crystal was 90°. In this orientation, the role of group velocity dispersion between the pump and the probe pulses becomes negligibly low. The calculations of group velocity mismatch between the pulses give values less than 9 fs/mm. For those calculations, we used Sellmeier equations, as in [17].

After passing through the crystal, the pump and the probe radiation entered the input slit of a homemade imaging spectrometer, which was placed 25 mm away from the output facet of the crystal. The spectrometer consisted of a flat, 300 lines/mm aluminum coated grating and two aberration-free objectives, which imaged the input slit onto a charge-coupled device (CCD) camera. The spectrometer was calibrated with a Hg lamp and the imaging properties were checked using a resolution test target. The spectral resolution in the vicinity of 405 nm was measured to be 3 nm. The spatial resolution along the slit within the spectral range of

*Corresponding author: rv_volkov@phys.msu.ru

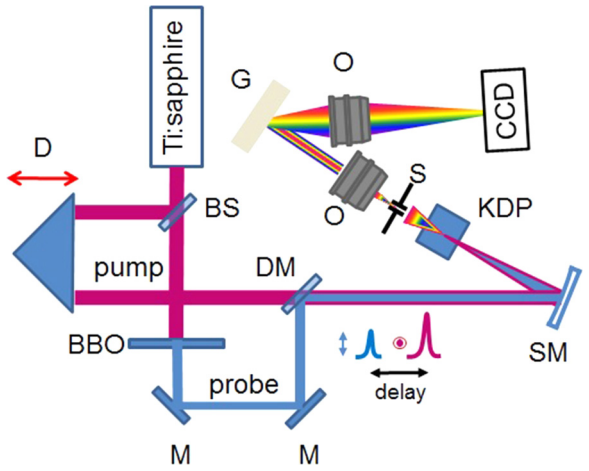

FIG. 1. (Color online) Experimental setup: D—delay line, BS—beam splitter, M—mirror, DM—dielectric mirror, SM—spherical mirror, BBO—frequency doubler, KDP—sample, S—slit, O—objective, G—grating, CCD—CCD camera.

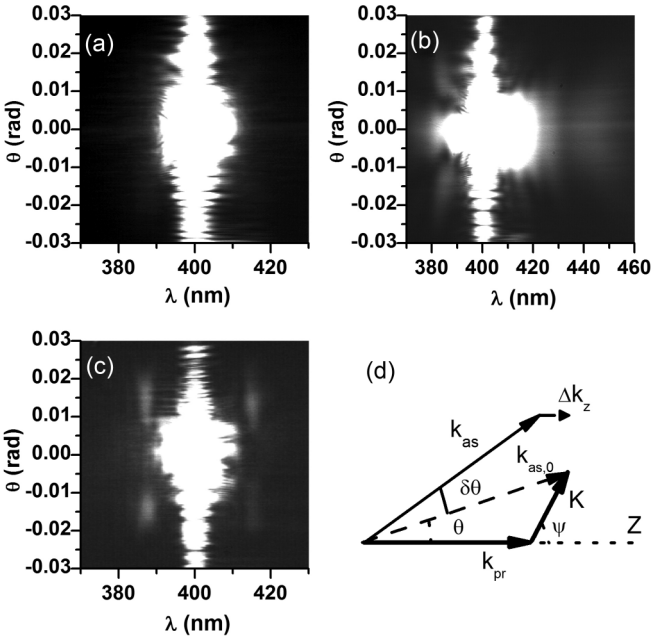

FIG. 2. Experimentally measured angularly resolved spectra of probe pulses at time delays of (a) −120 fs, (b) 0 fs, (c) 120 fs. θ is the angle inside the sample recalculated, considering the refraction at the crystal-air interface. (d) Vector diagram used for the phase-mismatching calculations for the anti-Stokes radiation; dashed vector $k_{as,0}$ is the wave vector of the anti-Stokes radiation oriented at the angle of the synchronism θ_0.

405–435 nm was better than 20 μm, which, in our geometry, corresponds to an angular resolution of 6×10^{-4} rad. The energy of the pump pulse at the sample was about 3 μJ—only slightly above the threshold for supercontinuum generation to be seen on the screen placed behind the target. At this level, a single filament was observed with no refocusing. The length L of the luminescing string, measured as described in [5], was about 0.6 mm and its starting point was situated about 4 mm from the entrance facet. As KDP is nonlinear crystal, it was verified that no SH signal was recorded by the CCD camera when the probe pulse was blocked.

We recorded a set of probe spectra at various delays. No noticeable spectral transformation of the probe signal was present at negative delays when the probe pulse arrived at the target before the pump pulse [Fig. 2(a)]. At delays comparable with the pulse duration, strong spectral broadening of the probe pulse was observed. The delay associated with the maximal spectral broadening was taken as zero delay [Fig. 2(b)]. For longer delays, two noticeable sidebands at wavelengths of about 400 ± 15 nm and at the angles of $\theta \approx \pm 0.015$ rad became visible [Figs. 2(c) and 2(d)]. These sidebands can be associated with the Stokes and anti-Stokes components generated by coherent scattering of the probe pulse by the pump pulse-induced A_1 phonon mode of KDP (frequency shift $\Omega \approx 915\,\mathrm{cm}^{-1}$ [16]). The measured decay time of the sidebands was 200 ± 40 fs, which corresponds to a dephasing time T_2 of about 400 ± 80 fs. This value agrees with that deduced from spectrometric measurements; using a Raman spectrometer (AvaRaman-785TEC), we measured the bandwidth of the 915 cm^{-1} Raman line to be $23 \pm 6\,\mathrm{cm}^{-1}$, which gives T_2 of 460 ± 120 fs.

III. RESULTS

The observed angular distribution of the Stokes and anti-Stokes radiation is ordinarily explained using phase-matching conditions [4]. It can be demonstrated that, in our experiments, the phase mismatch between the interacting waves that is accumulated over the filament length is too small. As a result, the bandwidth of an angular synchronism exceeds the cone angle of the scattered radiation, which is concentrated around $\theta \approx \pm 0.015$ rad [Fig. 2(c)].

Indeed, the maximal wave mismatch Δk for which the phase-matching condition is still fulfilled is $\Delta k \approx 0.9\pi/L$ (see, e.g., [17]), where L is the interaction length. The wave mismatch for anti-Stokes radiation calculated along the filament axis is given by the following expression [see Fig. 1(d)]: $\Delta k_z = k_{as}\cos(\theta_0 + \delta\theta) - k_{pr} - K\cos(\psi)$, where θ_0 is the angle of synchronism, $k_{pr} = \omega_{pr} n(\omega_{pr})/c$ and $k_{as} = \omega_{as} n(\omega_{as})/c$ are the wave vectors of the probe and anti-Stokes radiation, respectively; c is a speed of light; ω_{pr} and ω_{as} are the carrier frequencies of the probe and anti-Stokes pulses respectively; n is the refraction index at corresponding frequency, K is the length of the wave vector of the wake wave of the lattice vibrations, ψ is the angle at which it is oriented with respect to the filament axis z, and $\delta\theta$ is the angular detuning from the synchronism. For a small $\delta\theta$, $\Delta k_z \approx k_{as}\sin(\theta_0)\delta\theta$. Therefore, the angular bandwidth is $\Delta\theta = 2\delta\theta \approx 1.8\pi/[L k_{as}\sin(\theta_0)]$. For $k_{as} = 2\pi n(\omega_{as})/\lambda_{as}$, $L = 0.6$ mm, $\theta_0 = 0.015$ rad, $\lambda_{as} = 385$ nm, and $n(\omega_{as}) = 1.48$, it gives $\Delta\theta \approx 0.027$ rad. Meanwhile the angular width of the emission spots centered at $\theta_0 = \pm 0.015$ rad is about 0.005 rad [Fig. 2(c)]. Therefore, our measured ARS cannot be explained through phase-matching conditions formalism.

IV. MODELING AND DISCUSSION

To explain the measured ARS, we modeled the filamentation process using a modified nonlinear Schrödinger equation.

For slowly varying amplitude $A_p(z,r,\tau)$ in a frame moving at the group velocity $V_{gr} = (\partial\omega/\partial k)_{\omega 0}$ of the pump pulse, the equation takes the form (see, e.g., [18])

$$\frac{\partial A}{\partial z} = \frac{i}{2k_0}\hat{T}^{-1}(\Delta_\perp A) + i\hat{D}A + i\frac{2\pi k_0}{{n_0}^2}\hat{T}(P_{nl}) - i\frac{k_0}{2n_0N_{cr}}\hat{T}^{-1}(N_eA) - \frac{1}{2}N_e\sigma A - \frac{K\hbar\omega_0}{2}W\frac{A}{I}, \quad (1)$$

where $\tau = t - z/V_{gr}$ is retarded time. The terms of the right-hand side of Eq. (1) describe diffraction, dispersion, Kerr nonlinearity, plasma induced defocusing, inverse Bremsstrahlung absorption with cross section $\sigma = 3\times10^{-18}$ cm^2 [19–25], and K-photon absorption, respectively. The dispersion operator has the form: $\hat{D} = \sum_{m=2}^{\infty}(i^m k_m/m!)\partial^m/\partial\tau^m$, where $k_m = \partial^m k(\omega)/\partial\omega^m|_{\omega_0}$. Ionization rate W was calculated by the Keldysh formula [26] with a gap potential $U_i = 7.7$ eV [27]. $I = (cn_0/8\pi)|A|^2$ denotes the intensity of the pump; N_{cr} is a critical plasma density; $k_0 = \omega_0 n_0/c$, where ω_0 is the carrier frequency of the pump pulse, n_0 is a refraction index at frequency ω_0; and P_{nl} stands for the nonlinear polarization, which is divided into instantaneous and Raman parts: $P_{nl} = (n_0/2\pi)[n_2(1-\alpha)I + \Delta n_R]A$. The variation of the refraction index Δn_R, induced by the Raman nonlinearity, is set by the expression $\Delta n_R(z,r,\tau) = \alpha n_2\int_{-\infty}^{\tau} f(\tau - t')I(z,r,t')dt'$. The value of instant nonlinearity is characterized by $n_2 = 2.9\times10^{-16}$ cm^2/W [28], and coefficient $\alpha = 0.3$, which determines the balance between the fast and Raman nonlinearity components. The Raman response function can be expressed in the form $f(t) = [(T_2^2 + T_R^2)/(T_2^2T_R)]\exp(-t/T_2)\sin(2\pi t/T_R)$ [1], where $T_R = 36.5$ fs is the period of the oscillations, $T_2 = 400$ fs. Operator $\hat{T}$ has the form $\hat{T} = 1 + (i/\omega_0)\partial/\partial\tau$.

Equation (1) should be supplemented with an equation describing the evolution of the plasma density $N_e(z,r,\tau)$ [1]:

$$\frac{\partial N_e}{\partial\tau} = W + \frac{\sigma}{U_i}N_eI - \frac{N_e}{\tau_r}. \quad (2)$$

The first term on the right-hand side of Eq. (2) describes the field ionization contribution to free-electron generation, the second term accounts for avalanche ionization, and the third term represents electron recombination, with a characteristic time $\tau_r = 300$ fs [27]. The initial intensity distribution of the pump was taken to be Gaussian in both time and space with the FWHM duration and diameter of 50 fs and 90 μm, respectively.

The calculated Raman response wake wave was characterized by the wave vector **K**, amplitude $|\Delta n_R(\Omega)|$, and phase $\varphi_{n_R}(z,r)$ of the nonlinear refraction index change Δn_R, oscillating at the frequency Ω after the passing of the pump pulse. We found that the wave vector **K** of the calculated wake wave was oriented along the axis of the filament z, with a corresponding spatial period $\Lambda = 7.2\,u$m. The spatial distributions of $|\Delta n_R(z,r)|$ and $\varphi_{n_R}(z,r)$ are presented in Figs. 3(a) and 3(b), respectively. The distribution of $|\Delta n_R(z,r)|$ consists of several peaks separated by narrow "valleys" where $|\Delta n_R(z,r)|$ is minimal. This spatial behavior can be explained by the dynamics of the pump pulse splitting process, in which the initial pulse splits into two subpulses and the delay between these subpulses gradually increases [1]. Both the leading and the trailing subpulses excite Raman oscillations.

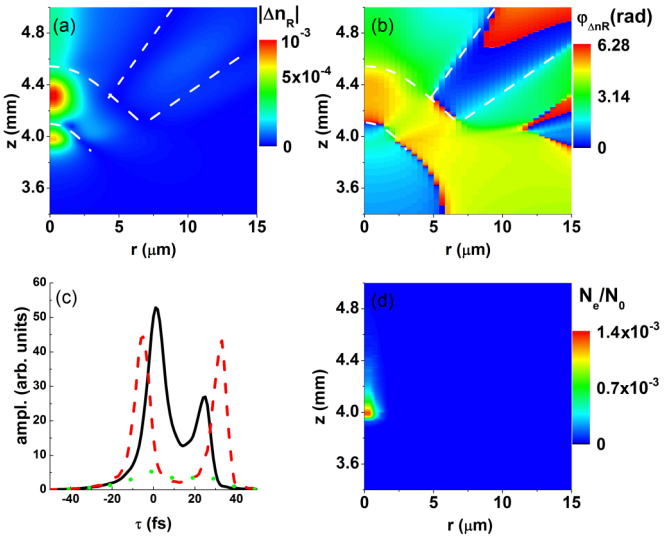

FIG. 3. (Color online) (a) Spatial distribution of the amplitude $|\Delta n_R(z,r)|$. (b) Spatial distribution of the phase $\varphi_{n_R}(z,r)$. (c) Intensity distribution of the pump pulse at $z = 4.1$ mm, $r = 0\,\mu$m (solid line); at $z = 3.9$ mm, $r = 4\,\mu$m (dotted line); and at $z = 4.3$ mm, $r = 0\,\mu$m (dashed line). (d) Spatial distribution of the normalized electrons concentration. Dashed lines in (a, b) indicate the position of the "valleys" of minimal $|\Delta n_R(z,r)|$.

The oscillations interfere constructively or destructively, depending on the relative phase. When the relative delay between the subpulses is equal to multiples of the oscillation period, nT_R, they interfere constructively and when the delay is equal to $(n + 1/2)T_R$, destructive interference occurs. Similarly, if the initial pulse splits into greater numbers of subpulses, the trailing subpulses dampen or amplify vibrations induced by the leading subpulses, depending on the delays. Indeed, as can be seen from Figs. 3(a) and 3(c),the minimal value of $|\Delta n_R(z,r)|$ at the axis of the filament in the vicinity of the first "valley" is observed at $z \approx 4.1$ mm when the delay between the subpulses is close to 18 fs ($T_R/2$). The maximum of $|\Delta n_R(z,r)|$ is reached at $z \approx 4.3$ mm when the delay is close to $T_R \approx 36.5$ fs. Similar coherent damping or amplification of molecular vibrations by the sequence of pulses is used in impulsive Raman spectroscopy [29] and for alignment of molecules [15]. Note that the positions of the maxima and minima of the $|\Delta n_R(z,r)|$ are not conditioned by the laser intensity modulation. To prove this, Fig. 3(d) shows the spatial distribution of the electron concentration N_e, which is determined mainly by the distribution of the intensity. The maximum value of the $|\Delta n_R(z,r)|$ is reached in the vicinity of $z \approx 4.3$ mm [Fig. 3(a)], while the maximum value of N_e is observed at $z \approx 4$ mm [Fig. 3(d)].

The calculated spatial distribution of the phase $\varphi_{n_R}(z,r)$ of the vibrational wake wave is presented in Fig. 3(b). From the comparison of Figs. 3(a) and 3(b), the phase of the vibrations changes by π rad in the vicinity of the "valleys" in $|\Delta n_R(z,r)|$. The dynamics of the pulse splitting process is different at the off-axis periphery and at the axis of the filament. For example, at $r = 4$ mm, the delay between the subpulses

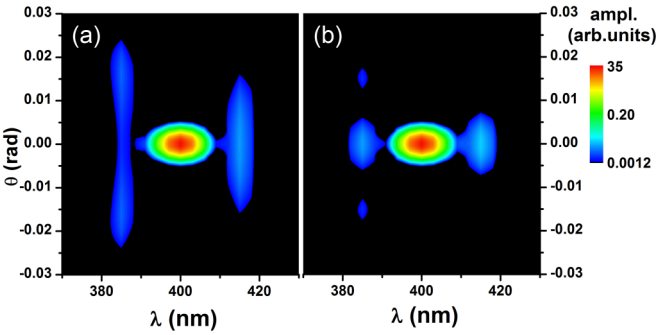

FIG. 4. (Color online) Calculated ARS formed by the probe radiation emitted from (a) the central part and (b) the periphery of the filament.

reaches $T_R/2$ at $z \approx 3.9$ mm, while at $r = 0$, the delay reaches $T_R/2$ at $z \approx 4.1$ mm [Fig. 3(b)]. This gives the "valleys" their bent shapes and indicates that the probe pulse can be simultaneously scattered by transversally separated areas with mutually antiphase lattice vibrations. It is worthwhile to note that the origins of the pulse splitting at the periphery and at the axis of the filament are different. While splitting at the axis of the filament arises from the interplay of group velocity mismatch and plasma formation [1], splitting at the off-axis periphery occurs because the intense central part of the pulse undergoes self-focusing and shifts towards the filament axis, leaving a gap in the intensity distribution. This gives the "valleys" their bent shapes and indicates that the probe pulse is simultaneously scattered by *transversally* separated areas with mutually antiphase lattice vibrations.

To confirm this idea, we numerically investigated the separate contributions of radiation scattered by the on-axis part of the filament and by its off-axis periphery to the total ARS of the probe pulse scattered by the filament. The angularly resolved spectrum amplitude $A(k_\perp,\omega)$ of the scattered probe

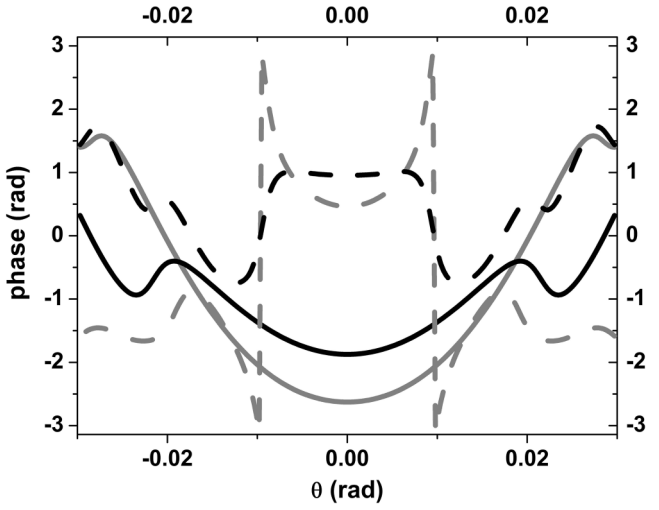

FIG. 5. Angular distribution of the phase of the anti-Stokes radiation at 385 nm (gray lines) and Stokes radiation at 415 nm (black lines) emitted from the center (solid lines) and the periphery (dashed lines) of the filament.

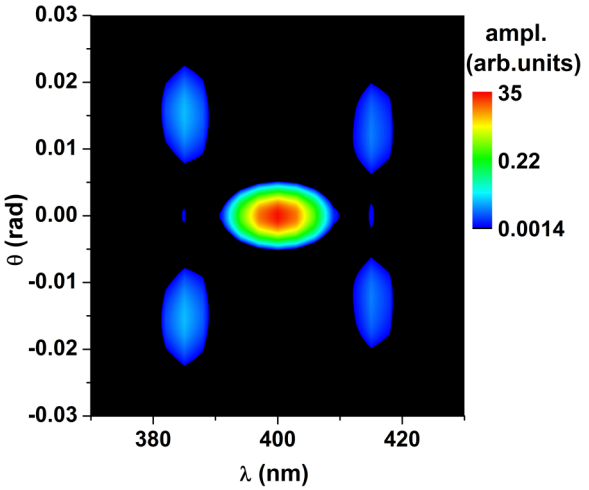

FIG. 6. (Color online) Calculated total ARS of the probe radiation as it exits the crystal.

radiation was calculated using the following formula [5,30]:

$$A_{s,as}(k_\perp,\omega) = i\frac{2\pi k(\omega)}{n(\omega)^2}\iint P_{s,as}(z,r,\omega)\exp(i\Delta k_{s,as}z)j_0(k_\perp r)2\pi r dr dz. \quad (3)$$

Indices "s" and "as" correspond to Stokes or anti-Stokes radiation. j_0 is the zero-order Bessel function, $\Delta k_{s,as}(\omega) = (\omega \pm \Omega)n(\omega \pm \Omega)/c - k(\omega)\cos(\theta), k(\omega) = \omega n(\omega)/c$, and $\theta = a\sin(k_\perp,/k)$.

Upper and lower signs relate to the Stokes or anti-Stokes radiation, respectively. Polarization amplitude at Stokes or anti-Stokes frequency is expressed in the form $P_{s,as}(z,r,\omega) = [n(\omega)/2\pi]|\Delta n_R(z,r)|\exp[i\varphi_{n_R}(z,r)]A_{pr}(r,\omega \pm \Omega)$, where A_{pr} is the spectral amplitude of the probe pulse.

Calculations were performed for the probe pulse with FWHM duration of 50 fs. The Rayleigh length of the probe beam with FWHM diameter of 45 μm exceeds 11 mm; therefore, it is assumed that the probe pulse diameter does not change with z.

The ARS of the scattered radiation emitted from the on-axis part of the filament ($0 < r < 5$ μm) and its off-axis periphery ($r > 5$ μm) are presented in Figs. 4(a) and 4(b), respectively. The ARS presented in Fig. 4(a) is almost isotropic.

Here, the cone angle $\Delta\theta$ of the emitted radiation is close to the value of the angular bandwidth which was estimated earlier in the Results section, based on the phase-matching conditions formalism.

Meanwhile the radiation scattered by the vast off-axis periphery propagates inside the small cone angle centered at $\theta \sim 0$ [Fig. 4(b)]. The comparison of the phase distributions, presented in Fig. 5, demonstrates that the emissions from the on-axis part of the filament and from its periphery are almost antiphase at $\theta \sim 0$. Owing to the resulting destructive interference, the total ARS of the probe pulse contains almost no emission at $\theta \sim 0$ (Fig. 6) and reproduces the experimentally observed ARS [Fig. 2(c)] very well.

V. CONCLUSIONS

In conclusion, the pump-probe scheme, with group velocity matched fundamental and second harmonic pulses, is applied for the investigation of the parameters of the wake wave of the Raman response, excited during filamentation of femtosecond radiation in the KDP crystal. We found that the trailing subpulse which originates from the pulse splitting of the pump coherently amplifies or dampens the lattice vibrations excited by the leading subpulse, depending on the delay between them. When the delay between the subpulses is equal to half of the oscillation period of lattice vibrations $T_R/2$, its amplitude reaches local minimal value while the phase of the wake wave "switches" by π rad. When reversed and the delay is equal to T_R the amplitude reaches maximum. As a consequence, the "field" of the lattice vibrations inside the filament consists of the areas with antiphase oscillations. The maximal amplitude of the wake wave is observed, not at the point with maximal intensity and electron concentration, but at the end of the filament—the place where the delay between the subpulses is equal to the period of the lattice vibrations. It confines the spatial coherence of the excited Raman wake wave. This effect should be observed if the initial pump pulse duration is comparable with the period of Raman oscillations of the media.

ACKNOWLEDGMENTS

This work was supported by the grant of the President of the Russian Federation for State Support of Leading Scientific Schools (Grant No. NSh-3796.2014.2) and by the Russian Foundation for Basic Research (Grant No. 15-02-99630a).

[1] A. Couairon and A. Mysyrowicz, Phys. Rep. **441**, 47 (2007).
[2] A. Brodeur and S. L. Chin, J. Opt. Soc. Am. B **16**, 637 (1999).
[3] S. Tzortzakis, L. Sudrie, M. Franco, B. Prade, A. Mysyrowicz, A. Couairon, and L. Bergé, Phys. Rev. Lett. **87**, 213902 (2001).
[4] D. Faccio, A. Dubietis, G. Tamosauskas, P. Polesana, G. Valiulis, A. Piskarskas, A. Lotti, A. Couairon, and P. Di Trapani, Phys. Rev. A **76**, 055802 (2007).
[5] R. V. Volkov, D. V. Khakhulin, and A. B. Savel'ev, Opt. Lett. **33**, 666 (2008).
[6] D. Uryupina, N. Panov, M. Kurilova, A. Mazhorova, R. Volkov, S. Gorgutsa, O. Kosareva, and A. Savelev, Appl. Phys. B **110**, 123 (2013).
[7] Y.-H. Chen, S. Varma, T. M. Antonsen, and H. M. Milchberg, Phys. Rev. Lett. **105**, 215005 (2010).
[8] J. K. Wahlstrand, Y.-H.Cheng, and H. M. Milchberg, Phys. Rev. A **85**, 043820 (2012).
[9] K. Hartinger, S. Nirmalgandhi, J. Wilson, and R. A. Bartels, Opt. Express **13**, 6919 (2005).
[10] F. Calegari, C. Vozzi, S. Gasilov, E. Benedetti, G. Sansone, M. Nisoli, S. De Silvestri, and S. Stagira, Phys. Rev. Lett. **100**, 123006 (2008).
[11] S. Varma, Y.-H. Chen, and H. M. Milchberg, Phys. Rev. Lett. **101**, 205001 (2008).
[12] H. Cai, J. Wu, H. Li, X. Bai, and H. Zeng, Opt. Express **17**, 21060 (2009).
[13] S. Varma, Y.-H. Chen, and H. M. Milchberg, Phys. Plasmas **16**, 056702 (2009).
[14] S. Varma, Y.-H. Chen, J. P. Palastro, A. B. Fallahkair, E. W. Rosenthal, T. Antonsen, and H. M. Milchberg, Phys. Rev. A **86**, 023850 (2012).
[15] J. P. Cryan, P. H. Bucksbaum, and R. N. Coffee, Phys. Rev. A **80**, 063412 (2009).
[16] M. K. Srivastava and C. H. Wang, J. Chem. Phys. **62**, 3439 (1975).
[17] V. G. Dmitriev, G. G. Gurzadyan, and D. N. Nikogosyan, *Handbook of Nonlinear Optical Crystals* (Springer-Verlag, Berlin,1999).
[18] J. Rolle, L. Bergé, G. Duchateau, and S. Skupin, Phys. Rev. A **90**, 023834 (2014).
[19] We applied the value which was used in [3] for the modeling of filamentation in fused silica, because it is unknown for KDP. This is reasonable because the electron collision time, which determines the cross-section value, is close for all transparent dielectrics, and for our regime of excitation is of the order of several femtoseconds [20–25]. Our calculations (not presented here) demonstrated that the variation of this time within this range did not lead to qualitative changes of the Raman wake wave behavior.
[20] M. D. Feit, A. M. Komashko, and A. M. Rubenchik, Appl. Phys. A **79**, 1657 (2004).
[21] Q. Sun, H. Asahi, Y. Nishijima, N. Murazawa, K. Ueno, and H. Misawa, Opt. Express **18**, 24495 (2010).
[22] V. V. Temnov, K. Sokolowski-Tinten, P. Zhou, A. El-Khamhawy, and D. von der Linde, Phys. Rev. Lett. **97**, 237403 (2006).
[23] A. Couairon, L. Sudrie, M. Franco, B. Prade, and A. Mysyrowicz, Phys. Rev. B **71**, 125435 (2005).
[24] Q. Sun, H. Jiang, Y. Liu, Z. Wu, H. Yang, and Q. Gong, Opt. Lett. **30**, 320 (2005).
[25] S. Quan, J. Hong-Bing, L. Yi, Z. Yong-Heng, Y. Hong, and G. Qi-Huang, Chin. Phys. Lett. **23**, 189 (2006).
[26] L. V. Keldysh, Sov. Phys. JETP **20**, 1307 (1965).
[27] G. Duchateau, G. Geoffroy, A. Dyan, H. Piombini, and S. Guizard, Phys. Rev. B **83**, 075114 (2011).
[28] A. J. Taylor, G. Rodriguez, and T. S. Clement, Opt. Lett. **21**, 1812 (1996).
[29] A. M. Weiner, D. E. Leaird, G. P. Wiederrecht, and K. A. Nelson, J. Opt. Soc. Am. B **8**, 1264 (1991).
[30] M. Kolesik and J. V. Moloney, Phys. Rev. E **70**, 036604 (2004).